Eur J Nucl Med Mol Imaging
DOI 10.1007/s00259-009-1135-8

ORIGINAL ARTICLE

Radiation dosimetry and biodistribution of ^{99m}Tc-ethylene dicysteine-deoxyglucose in patients with non-small-cell lung cancer

Naomi R. Schechter · William D. Erwin · David J. Yang · E. Edmund Kim · Reginald F. Munden · Kenneth Forster · Lina C. Taing · James D. Cox · Homer A. Macapinlac · Donald A. Podoloff

Received: 19 September 2008 / Accepted: 23 March 2009

Abstract
Purpose To assess the radiation dosimetry and biodistribution of ^{99m}Tc-labeled ethylene dicysteine deoxyglucose (^{99m}Tc-EC-DG) in patients with non-small-cell lung cancer (NSCLC).
Methods Serial whole-body scans were acquired 0, 2, 4, 6 and 24 h after injection of ^{99m}Tc-EC-DG (925 MBq) in seven NSCLC patients. Radiation dosimetry, blood clearance and SPECT imaging of the primary tumor were assessed.
Results The critical organ was the bladder wall, with average radiation absorbed dose over all seven patients of 2.47×10^{-2} mGy/MBq. The average effective dose equivalent and effective dose were 6.20×10^{-3} mSv/MBq (6.89 mSv/1,110 MBq) and 5.90×10^{-3} mSv/MBq (6.54 mSv/1,110 MBq), respectively. The primary tumor was visualized with SPECT in six patients. On final pathology, one patient had a granuloma, which did not enhance with ^{99m}Tc-EC-DG.
Conclusion ^{99m}Tc-EC-DG has acceptable dosimetric and biodistribution properties as a diagnostic tumor-imaging agent. Future studies are planned to evaluate its diagnostic potential.

Keywords EC-DG · Lung cancer · SPECT · Glucosamine · Deoxyglucose

N. R. Schechter · K. Forster · L. C. Taing · J. D. Cox
Division of Radiation Oncology,
The University of Texas M. D. Anderson Cancer Center,
Houston, TX 77030, USA

W. D. Erwin · D. J. Yang · E. E. Kim · R. F. Munden · H. A. Macapinlac · D. A. Podoloff
Division of Diagnostic Imaging,
The University of Texas M. D. Anderson Cancer Center,
Houston, TX 77030, USA

N. R. Schechter (✉)
Department of Radiation Oncology,
UCSF Helen Diller Family Comprehensive Cancer Center,
The University of California, San Francisco,
1600 Divisadero, Suite H1031,
San Francisco, CA 94143-1708, USA
e-mail: nschechter@radonc.ucsf.edu

Introduction

We report here the radiation dosimetry and biodistribution of ^{99m}Tc-labeled ethylene dicysteine deoxyglucose (^{99m}Tc-EC-DG) in patients with non-small-cell lung cancer (NSCLC).

Imaging the tumor accumulation of ^{18}F-FDG with a PET scan has proven quite useful in the identification of malignant tumors [1, 2]. It has even been recommended that ^{18}F-FDG PET data be integrated into planning of radiation therapy for NSCLC, particularly for three-dimensional conformal techniques [3, 4]. Unfortunately, a significant amount (>95%) of ^{18}F-FDG concentrates in the cytosolic fraction, which results in false-positive findings and difficulty distinguishing between inflammation or infection and tumor [5–8].

Our goal was to develop a noninvasive, single photon emission CT (SPECT) glucose metabolism imaging agent that could potentially detect NSCLC tumors more specifically than ^{18}F-FDG PET. For this purpose, we developed and conjugated ethylenedicysteine (EC) with deoxyglucose (DG), and labeled the resulting agent, EC-DG, with ^{99m}Tc [9]. The molecular structure of ^{99m}Tc-EC-DG is shown in Fig. 1.

Published online: 25 April 2009

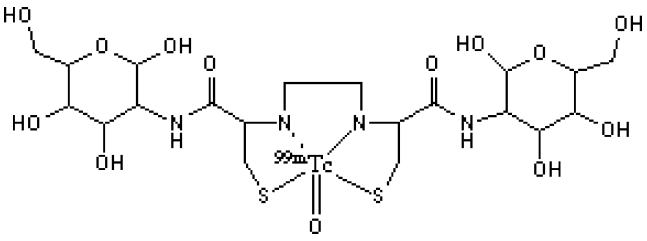

Fig. 1 Structure of ^{99m}Tc-EC-DG

The molecule EC-DG has key position(s) available for interaction(s). For example, D-glucosamine can be acetylated and phosphorylated at positions 2 and 6. EC has two COO– arms and the two dithiol (SH) locations. During synthesis, the molecule changes to a peptide linkage with two glucosamine arms, with EC linked at position 2 at both sites of the glucosamine. EC retains two dithiols that can react with glycoproteins and the lumen of the cell membrane, such as *O*-linked *N*-acetylglucosamine [10–13]. It is likely that S–H bonds of EC-DG bind to cytosolic and transmembrane enzymes (beta-*N*-acetylglucosaminidase and *O*-GlcNAc transferase) or membrane-associated proteins (*O*-linked *N*-acetylglucosamine) which form (EC-DG)S–S(protein) linkages (docking and fusion) and support the translocation of EC-DG into the cell nucleus. It is known that glucosamine is phosphorylated at positions 1 and 6 and binds with uridine diphospho-*N*-acetylglucosamine to form *O*-linked *N*-acetylglucosamine at those same positions that involve nuclear and cytosolic protein interactions. Recent studies demonstrate a role for *O*-GlcNAcylation in processes as diverse as transcription in the nucleus and signaling in the cytoplasm, suggesting that *O*-GlcNAc has both protein and site-specific influences on biochemistry and metabolism throughout the cell [10, 11].

Preclinical work evaluating the feasibility of ^{99m}Tc-EC-DG imaging in tumor-bearing rodents has been previously published [9, 14, 15]. In these studies, EC-DG was positive for phosphorylation in the hexokinase assay: blood glucose levels increased following EC-DG injection and decreased after insulin administration. Scintigraphic results have demonstrated the feasibility of ^{99m}Tc-EC-DG imaging. Tumor-to-brain tissue and tumor-to-muscle tissue ratios of ^{99m}Tc-EC-DG uptake were higher than those of ^{18}F-FDG uptake, likely due to the overall hydrophilicity and unique cell internalization properties of ^{99m}Tc-EC-DG. Based on the promising preclinical findings, the US Food and Drug Administration (FDA) approved a phase I study in humans. This article is the first report of the radiation dosimetry and biodistribution of ^{99m}Tc-EC-DG in human subjects. The results of SPECT imaging of the primary tumor are also reported briefly.

Materials and methods

Synthesis and labeling of ^{99m}Tc-EC-DG

^{99m}Tc-EC-DG was prepared as described previously [9]. All clinical samples were tested for radiochemical purity (AR-2000 radio-TLC scanner; Bioscan, Washington, DC), sterility and pyrogenicity (South Texas Nuclear Pharmacy, Houston, TX).

Synthesis of EC-DG has been previously reported [9]. Briefly, EC was dissolved in $NaHCO_3$. To this colorless solution were added sulfo-*N*-hydroxysuccinimide (sulfo-NHS) and 1-ethyl-3-(3-dimethylaminopropyl) carbodiimide-HCl (EDAC) (Aldrich Chemical Co., Milwaukee, WI). D-Glucosamine hydrochloride salt (Sigma Chemical Co., St. Louis, MO) was then added. A pH of 8 was measured. The mixture was stirred at room temperature for 16 h and then dialyzed for 24 h using Spectra/POR molecular porous membrane with cut-off at 500 Da (Spectrum Medical Industries, Houston, TX). After dialysis, the product was filtered through a 0.45-μm nylon filter and then freeze-dried using a lyophilizer (Labconco, Kansas City, MO). EC-DG was labeled with ^{99m}Tc in the presence of tin(II) chloride. ^{99m}Tc was chelated in the EC core.

Two assays, thin-layer chromatography (TLC) and high-performance liquid chromatography (HPLC), were used to determine radiochemical purity. The TLC chromatogram (ITLC-SG) was scanned for distribution of radioactivity in a radiochromatogram scanner. Using 1 *M* ammonium acetate/methanol (4:1) or saline elution, the retardation factor (Rf) of ^{99m}Tc-EC-DG was 0.8. For the HPLC assay, ^{99m}Tc-EC-DG (20 μl, 1 mg/ml EC-DG) was loaded onto a C-18 reverse-phase column (Waters, semi-prep, 7.8×300 mm) and eluted with water at a flow rate of 0.5 ml/min. UV absorbance at 210 nm or 272 nm was used to assess the purity of ^{99m}Tc-EC-DG; UV at 210 nm is preferred. We accept a radiochemical purity of greater than or equal to 90% as a specification for the drug product.

For the pyrogenicity assay, a gel clot LAL lysate kit (Sigma Chemical Company, St. Louis, MO) with a sensitivity of 0.125 *E. coli* units (EU) per milliliter was used to determine bacterial endotoxins. Drug solution (0.1 ml) was incubated in vials for 1 h at room temperature. Pyrogenicity was assayed by visualizing the gel clot in the solution to ensure no more than 175 EU per 4 ml of the drug injection, in which 1 ml is the maximum recommended total dose at the expiration time. To ensure sterility, each batch of product was tested using culture vials with aerobic and anaerobic materials (NR6 and NR7; Becton Dickinson Diagnostic Instrument Systems, Towson, MD). Drug solution (0.3 ml) was incubated in Bactec culture vials for 7 days at 37°C. Sterility was assayed by visualizing the cloudiness of the solution.

Study approval

This study (MDACC ID01-415) was approved by the M. D. Anderson Cancer Center clinical research committee, institutional review board, radioactive drug research committee, and radiation safety committee. It was also approved by the FDA under (IND) application 63698 held by Cell>Point LLC (Englewood, CO). The phase I clinical trial (RO00-311) opened for patient accrual on 30 January 2003. All patients gave their informed consent.

Patient eligibility

Each eligible patient had to be an adult (18 years of age or older), and have a pathologic diagnosis of NSCLC with no pathologic evidence of small-cell or bronchioloalveolar carcinoma of the lung. There was no tumor stage restriction. None of the patients had undergone mediastinoscopy, fine-needle aspiration of a mediastinal node, or biopsy of a mediastinal node. None of the patients had received radiation therapy to the chest. None of the patients had received chemotherapy or other treatment for this or any other lung cancer. Pleural effusion on the most recent chest radiograph was cause for exclusion. In addition, a patient was excluded if he or she had a history of: any other primary cancer, renal insufficiency, hepatic insufficiency, insulin-dependent diabetes mellitus, or a myocardial infarction in the 6 months prior to evaluation for study participation. Patients with a history of skin cancer, carcinoma in situ of the cervix, or other tumors that had been in remission for 2 years or longer were considered eligible.

The FDA recommended the use of ^{18}F-FDG PET findings as the gold reference standard for comparison of SPECT findings, since our subjects were to be imaged with ^{99m}Tc-EC-DG before candidacy for definitive surgery was determined. Therefore, as part of the standard evaluation, each patient must have had, or have planned or scheduled within 14 days of consent, an ^{18}F-FDG PET/CT scan at our institution. A CT scan of the chest with contrast agent administration had to be planned, scheduled, or to have been completed within 30 days of study consent. As part of the standard evaluation, chest radiography (with anterior-posterior and lateral views), magnetic resonance imaging (MRI) or CT scan of the brain with contrast agent administration (when clinically indicated), and a bone scan (when clinically indicated) must have been performed within 30 days prior to the patient's consent or planned (not necessarily scheduled) within a 2-week period after consent to this study. Inability to lie flat and remain still for 45 min was an exclusion criterion.

Criteria for removal from the study

Criteria for removal from the study included: (1) patient noncompliance with protocol requirements, (2) unacceptable adverse reaction, (3) patient's wishes, (4) belief that the constraints of the study were detrimental to the patient's health, and (5) inpatient status on day(s) planned for the ^{99m}Tc-EC-DG scans.

^{99m}Tc-EC-DG imaging

Each patient fasted for at least 8 h prior to the administration of ^{99m}Tc-EC-DG. The last meal before this fast was recommended to be high in protein and low in carbohydrates. Only high-protein low-carbohydrate snacks were allowed from the time of ^{99m}Tc-EC-DG injection until all of the patient's whole-body and SPECT study images were acquired.

Prior to ^{99m}Tc-EC-DG administration, anterior whole-body planar transmission scans of a ^{57}Co sheet source placed on the posterior detector of a dual-head gamma camera equipped with low-energy high-resolution (LEHR) collimators (E.Cam, Siemens Medical Solutions USA, Hoffman Estates, IL) were acquired at a 10 cm/min scan speed both without and with the patient in between, for attenuation correction of the geometric mean regional count data from the whole-body planar ^{99m}Tc-EC-DG scans. Approximately 925 MBq (25 mCi) of ^{99m}Tc-labeled EC-DG was then injected as a bolus via an antecubital vein, with the patient lying on the imaging table, followed immediately by a 5-ml flush of isotonic saline solution. Simultaneous anterior-posterior whole-body planar scans were acquired immediately after injection, and then at 2, 4 and 6 h, at a scan speed of 10 cm/min. (The first four patients were also scanned at 24 h, but a statistical comparison between residence times calculated with and without the 24-h scan was performed prior to the fifth patient, which demonstrated that the 24-h scan could be eliminated.) The immediate postinjection scan was acquired prior to micturition, to ensure the total-body image at t=0 h contained 100% of the administered activity.

SPECT scanning of the thorax including the primary tumor was also performed after each of the 2-, 4- and 6-h whole-body scans. The acquisition parameters for each SPECT scan were: LEHR collimation, 120 step-and-shoot views over 360° (60 views per head), 180° noncircular orbit rotation, 128×128 image matrix with a zoom factor of 1 (4.8 mm/pixel sampling), and 26 s per view (30 min total scan time, accounting for the 4-s step time between views). Each SPECT scan was reconstructed iteratively (10 subsets, 12 iterations, and two-pixel-wide [9.6 mm FWHM] 3-D gaussian post-filtering), employing an algorithm that incorporated attenua-

tion correction based on the CT scan derived from the PET/CT study that was manually registered to the SPECT, as well as compensation for the system resolution of the gamma camera. Both the PET/CT and SPECT scans were acquired with the patient positioned in a customized radiation therapy immobilizer, and seven fiducial markers (^{57}Co spot markers, visible on both SPECT and CT) were placed on the sternal notch, clavicles and sides to aid in the task of manual registration. The reconstructed slices were visually assessed for the presence of ^{99m}Tc-EC-DG in the primary tumor.

The degree of agreement between the two imaging techniques, ^{99m}Tc-EC-DG and ^{18}F-FDG PET, was measured, with ^{18}F-FDG PET results serving as the reference standard. If pathologic specimens from the thorax were obtained within 4 weeks following administration of ^{99m}Tc-EC-DG, then that pathologic information was compared with the ^{99m}Tc-EC-DG and ^{18}F-FDG PET scan results. The ^{99m}Tc-EC-DG scans were reviewed blindly and independently by a single physician certified by the American Board of Nuclear Medicine and the American Board of Radiology (as a diagnostic radiologist with special competence in nuclear radiology). The reference ^{18}F-FDG PET scans were reviewed blindly and independently by another single physician certified by the American Board of Nuclear Medicine. The diagnostic chest CT scans to be used as reference for tumor volumes on this study were reviewed by consensus of two other physicians certified by the American Board of Radiology. Thoracic pathology findings to be used for comparison with ^{99m}Tc-EC-DG and ^{18}F-FDG PET scan findings in this study were reviewed by a single physician certified by the American Board of Pathology.

A tumor-to-background (T:B) ratio was calculated for each ^{99m}Tc-EC-DG SPECT and ^{18}F-FDG PET scan, for quantitative comparison of tumor uptake. The T:B ratio was computed from two-dimensional regions of interest (ROIs) defined on a transverse slice through the center of the tumor on each scan. A ROI was manually defined around the tumor, and then a duplicate was generated to serve as the background ROI. The background ROI was mirrored over normal tissue in the contralateral lung, unless the contralateral region included non-lung tissue (e.g., upper liver, blood pool, soft tissue), in which case a nonmirrored region in the ipsilateral lung was used instead. The T:B ratio was calculated as the ratio of the tissue count density (^{99m}Tc-EC-DG SPECT) or average SUV (^{18}F-FDG PET) in the two ROIs.

Radiation dosimetry of ^{99m}Tc-EC-DG

Radiation absorbed doses to organs from ^{99m}Tc-EC-DG were estimated from geometric mean quantification of the total-body and organ activities in the serial whole-body planar emission images. For all imaging time points, ROIs were manually drawn around the whole body, and each organ with visible uptake, on both the anterior and posterior scans. The organs included the kidneys, liver, lungs, spleen, stomach, testes, thyroid, and urinary bladder contents. A background ROI near each organ was also defined in order to be able to subtract superimposed extra-organ activity. Total background-corrected counts within each anterior and posterior ROI were calculated, and their geometric mean was then computed [(anterior counts × posterior counts)$^{1/2}$] [15, 16]. The geometric mean of the total counts was corrected for attenuation using the measured counts from the same region in the transmission scans without and with the patient. The multiplicative attenuation correction factor for the geometric mean quantitative method is the square root of the region without-to-with count ratio, raised to the power μ_{140}/μ_{122} to convert from ^{57}Co to ^{99m}Tc attenuation, where μ_{140} and μ_{122} are the mass attenuation coefficients for ^{99m}Tc and ^{57}Co, respectively. Finally, the attenuation-corrected counts were converted to fraction of injected activity by dividing by the administered activity and the camera sensitivity (counts per microcurie) measured with a reference source of known ^{99m}Tc activity in a 10-ml vial acquired in each patient whole-body scan.

For all organs except the bladder, the residence time was calculated from the integral of either a single or biexponential function that had been fitted to the least-squares fit of the estimated fraction of injected activity as a function of time. The residence time for the bladder was estimated using the Medical Internal Radiation Dose (MIRD) dynamic bladder model with a 2-h voiding interval and a single or biexponential fit of the remainder of the body (total minus all organs) plus bladder contents fraction of injected activity versus time as the input function. The choice of a 2-h voiding interval was based on the requirement that the patient void immediately before each of the 2-, 4- and 6-h whole-body scans. The use of the remainder of the body plus bladder contents activity as the input function was based on the reasonable assumption that excretion of ^{99m}Tc-EC-DG is predominantly urinary, and all EC-DG not accumulated in the organs would eventually be excreted in the urine. Radiation absorbed dose estimates were calculated using the MIRD methodology. The residence times were entered into the MIRDOSE version 3.1 personal computer program for implementation of the MIRD absorbed dose calculations, and the resulting unit absorbed dose, effective dose equivalent and effective dose estimates were tabulated [17–20].

Blood clearance

Blood samples (2 ml volume) were collected from all patients at approximately 5, 15, 20, 30 and 45 min, and 1, 2, 4, 6 and

Table 1 Absorbed dose for each target organ

Target organ	Absorbed dose (mGy/MBq, mean±SD)
Adrenals	0.0033±0.0009
Brain	0.0015±0.0007
Breasts	0.0016±0.0005
Gallbladder	0.0034±0.0010
Lower large intestine	0.0033±0.0009
Small intestine	0.0029±0.0008
Stomach	0.0084±0.0071[a]
Upper large intestine	0.0029±0.0009
Heart wall	0.0028±0.0009
Kidneys	0.0123±0.0037
Liver	0.0047±0.0017
Lungs	0.0056±0.0009
Muscle	0.0021±0.0006
Ovaries	0.0041±0.0005
Pancreas	0.0039±0.0015
Red marrow	0.0022±0.0007
Bone surfaces	0.0036±0.0012
Skin	0.0013±0.0005
Spleen	0.0045±0.0023[a]
Testes	0.0067±0.0029
Thymus	0.0021±0.0008
Thyroid	0.0063±0.0031[a]
Urinary bladder	0.0247±0.0090
Uterus	0.0053±0.0006
Total body	0.0024±0.0007
Effective dose equivalent (mSv/MBq[b])	0.0062±0.0007
Effective dose (mSv/MBq[c])	0.0059±0.0011

[a] Based on doses in all seven patients, including patients with no uptake in the organ (one for stomach and thyroid; three for spleen).

[b] ICRP Publication 26, 1977.

[c] ICRP Publication 60, 1990.

24 h after injection of ^{99m}Tc-EC-DG. A baseline sample was also drawn from each patient approximately 30 min before injection of ^{99m}Tc-EC-DG. The times of the actual sample collections were recorded and used for data analysis. Aliquots (100 μl) were drawn from each blood sample and radioactivity was assayed using a Cobra II gamma counter (Packard Instrument Co., Meriden, CT). Data were recorded as counts per minute with decay correction, to allow assessment of biologic clearance from the blood. A calibration standard of equivalent volume was counted for conversion from counts per minute to microcuries. The data are expressed as percentage of injected dose per gram of blood.

Safety

Vital signs including heart rate, respiratory rate, blood pressure and temperature were monitored at four time points: approximately 1.5 h before and 1, 4, and 17–24 h after the bolus injection of ^{99m}Tc-EC-DG. Samples for potassium, calcium, and magnesium levels were drawn at three time points: approximately 1 h before, 10 min before, and 80 min after the bolus injection of ^{99m}Tc-EC-DG. Twelve-lead electrocardiography (ECG) was performed at three time points: approximately 1 h before, time 0, and 1.5 h after the bolus injection of ^{99m}Tc-EC-DG. At the time of each ECG, patient symptoms and medications were documented as well. A board-certified cardiologist inter-

Table 2 Source organ residence times

Source organ	Residence time (h, mean±SD)
Stomach	0.22±0.21[a]
Kidneys	0.21±0.07
Liver	0.25±0.12
Lungs	0.28±0.05
Spleen	0.03±0.02[b]
Testes	0.02±0.01[b]
Thyroid	0.01±0.004[a]
Urinary bladder contents	0.47±0.15
Remainder	2.78±1.07

[a] Greater than zero in only six of seven patients.

[b] Greater than zero in only four of seven patients (testes only applicable to the four male patients).

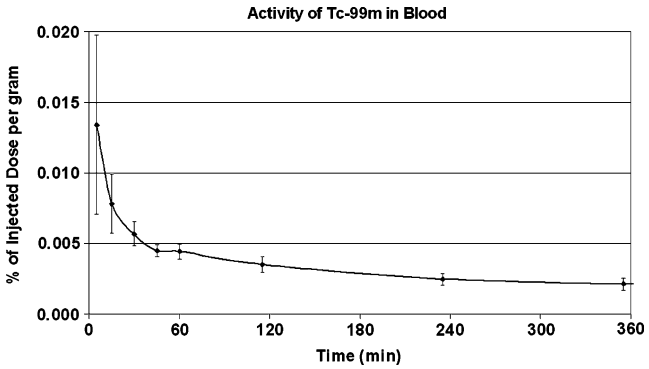

Fig. 2 The composite time–activity curve for ^{99m}Tc-EC-DG in blood for all seven patients. The percentage of the injected dose per gram of blood (%ID/g) is presented as a function of the time elapsed since injection of ^{99m}Tc-EC-DG. The plot extends only out to 6 h, to better separate the high density of data points within the first hour

preted these findings. Each patient was also observed for dermatologic reactions such as bruising, allergic reactions/hypersensitivity, and wound infection immediately after injection of ^{99m}Tc-EC-DG and then approximately 1, 3, and 5 h later. Patients were also contacted by a nurse approximately 96 h after injection of ^{99m}Tc-EC-DG to report any adverse reactions that may have occurred in the interim.

Results

Total number of patients

The clinical trial was closed after 16 months (24 May 2004) and the available data and results from the seven patients treated with ^{99m}Tc-EC-DG (four men and three women; median age 69 years, range 52–78 years) were submitted to the FDA for review.

Radiation dosimetry

Target organs The organ estimated to receive the highest dose was the bladder wall, with an average absorbed dose among the seven patients of 2.47×10^{-2} mGy/MBq (9.12×10^{-2} rad/mCi). The kidneys were estimated to receive the second highest absorbed dose, 1.23×10^{-2} mGy/MBq (4.56×10^{-2} rad/mCi). Table 1 shows the average and standard deviation (SD) of absorbed dose for all target organs calculated over all seven patients. Average and SD of residence time for the defined source organs of activity and the remainder of the body are tabulated in Table 2.

Effective dose equivalent and effective dose The mean effective dose equivalent over all seven patients was 6.20×10^{-3} mSv/MBq, or 6.89 mSv for administration of 1,110 MBq (30 mCi) activity, and the mean effective dose was 5.90×10^{-3} mSv/MBq, or 6.54 mSv for 1,110 MBq (30 mCi).

Blood clearance

An average blood time–activity curve was calculated from the pooled blood sample data of all seven patients (Fig. 2). The clearance of ^{99m}Tc-EC-DG from the blood was rapid and biphasic, dropping below 0.005% of the administered activity by 1 h after injection.

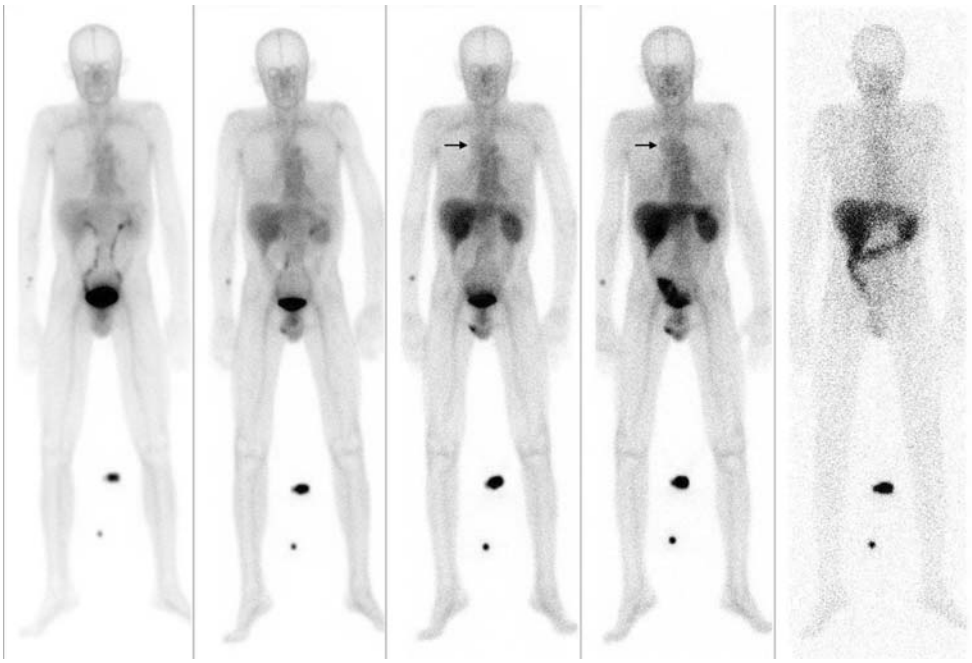

Fig. 3 Anterior whole-body images of ^{99m}Tc-EC-DG in a patient with NSCLC in the right upper lung (*arrow*), obtained after administration of 925 MBq (25 mCi). The images were acquired (*from left to right*) immediately, and 2, 4, 6 and 24 h after injection. Each image is self-normalized for display for better visualization of the biodistribution at each time point

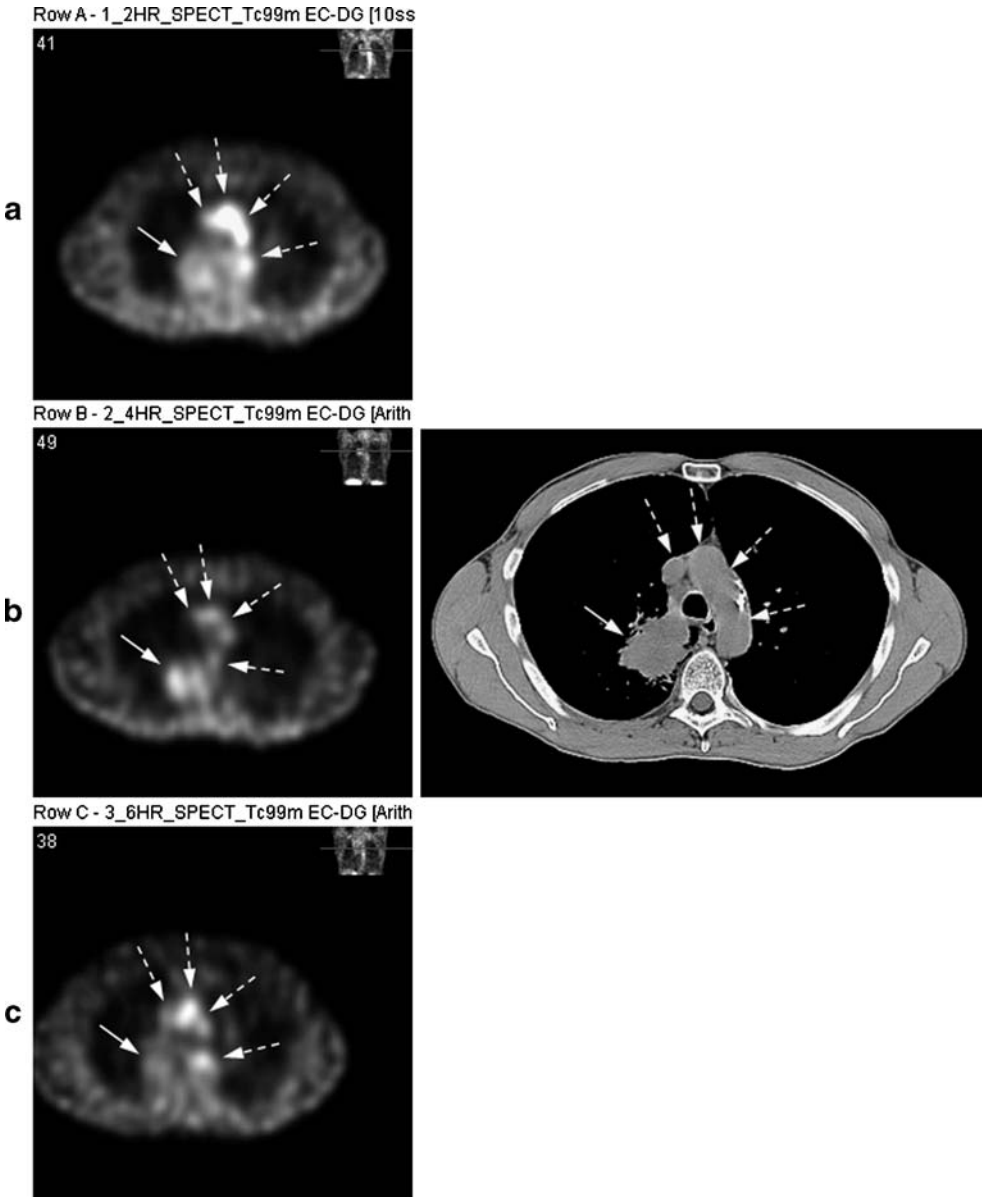

Fig. 4 CT attenuation-corrected SPECT transverse slices obtained after administration of 925 MBq (25 mCi) of ^{99m}Tc-EC-DG in a patient with NSCLC in the medial posterior right upper lung (*solid arrow*). Uptake is also seen in the blood pool (great vessels, *dashed arrows*). The three images (*left*, *from top to bottom*) are from the 2-, 4- and 6-h SPECT scans, respectively (*right* reference CT slice shown for anatomical correlation)

Safety

None of the patients suffered a serious adverse event related to the ^{99m}Tc-EC-DG. One patient developed minimal erythema at the injection site which self-resolved within an hour. No vital sign, electrolyte or ECG abnormality was attributed to the administration of ^{99m}Tc-EC-DG.

Biodistribution – whole-body scans

Uptake of ^{99m}Tc-EC-DG was visualized primarily in the blood pool, kidneys, bladder and liver in all seven patients. Uptake was also seen secondarily in the stomach (six patients), thyroid (six patients), testes (all four male patients), spleen (four patients) and gastrointestinal tract (mostly in the 6- to 24-h images). The primary lung lesion

Table 3 ^{99m}Tc-EC-DG SPECT and ^{18}F-FDG PET T:B uptake ratios

Patient	^{99m}Tc-EC-DG			^{18}F-FDG
	2-h	4-h	6-h	
1	3.49	4.19	4.24	29.48
2	4.87	6.62	3.68	29.63
3	2.61	2.83	3.22	18.61
4[a]	3.76	–	2.95	11.79
5[b]	–	3.85	–	19.84
6	2.53	2.54	3.67	13.54

[a] SPECT scans acquired at 2, 6 and 7.5 h (no 4-h scan, and 7.5-h scan was excluded).

[b] SPECT scan at 4 h.

was visualized on planar whole-body scanning in four patients. No uptake was visualized in either the brain or the myocardium in any of the seven patients. The biodistribution of ^{99m}Tc-EC-DG over time in a representative patient is illustrated in Fig. 3.

Tumor uptake – SPECT imaging

The primary tumor was grossly visualized with ^{99m}Tc-EC-DG SPECT in six of the seven patients, with the 4-h SPECT scan generally providing the highest contrast relative to the surrounding tissue (Fig. 4). The ^{18}F-FDG-PET scan of the primary tumor was positive in all seven patients. All of the patients were reported to have primary NSCLC on the biopsy specimen. On lobectomy, one patient (for whom ^{18}F-FDG PET was positive and ^{99m}Tc-EC-DG SPECT was negative) was pathologically documented to have histoplasma capsulatum with a necrotic calcified granuloma; initial biopsy of the site was falsely positive. Evidence of anthrasis and an old fibrotic granuloma were found in the patient's mediastinum.

A patient-by-patient comparison of T:B ratios between the 2-, 4- and 6-h ^{99m}Tc-EC-DG SPECT and ^{18}F-FDG PET scans for the six patients with tumor uptake of ^{99m}Tc-EC-DG is shown in Table 3. The T:B ratios were (mean±SD) 3.45±0.96, 4.01±1.61, 3.55±0.49 and 20.48±7.65, for the 2-, 4- and 6-h ^{99m}Tc-EC-DG SPECT and ^{18}F-FDG PET scans, respectively.

The granuloma enhanced on the ^{18}F-FDG PET scan, with a T:B ratio of 7.94. The granuloma showed no uptake on the 2-, 4-, and 6-h ^{99m}Tc-EC-DG SPECT scans, with T:B ratios of 0.99, 1.02, and 0.96, respectively .

Discussion

Radiation dosimetry and pharmacokinetics

The biodistribution of ^{99m}Tc-EC-DG showed its major route of excretion to be through the kidneys (Fig. 3). The compound has a very low molecular weight (591 Da) and was rapidly cleared from the blood, as shown by the plasma time–activity curve (Fig. 2). Nontarget tissues exhibited rapid washout of the tracer resulting in increasing T:B count density ratios over time.

The presence of multiple hydroxyl groups makes the compound highly hydrophilic. This hydrophilicity increases its renal clearance. The hydrophilicity also limits passive diffusion of ^{99m}Tc-EC-DG through cell membranes, leading to our hypothesis that the accumulation seen in tissues is related to active transport through transporters, receptors, or molecular interactions between EC sulfhydryl groups and cell-associated proteins. The hydrophilicity may also prevent ^{99m}Tc-EC-DG from freely crossing membranes such as the blood–brain barrier, and limit accumulation of ^{99m}Tc-EC-DG in normal brain tissue. We have previously reported that tumor uptake of ^{99m}Tc-EC-DG is most likely via a process related to glucose metabolism [9, 14]. It should be noted, however, that there are at least five glucose transporters. Glucose transporters 1 and 3 are localized in brain tissue. Poor brain uptake of radiolabeled glucosamine has been also reported by others [21]. The observation that uptake of ^{99m}Tc-EC-DG is low in the brain and heart of human subjects increases the possibility for metal-therapeutic and radio-therapeutic applications of EC-DG.

Safety and clinical findings

Imaging of primary NSCLC tumors with 9.25×10^{2} MBq (25 mCi) of ^{99m}Tc-EC-DG appears to be feasible and safe. The effective dose equivalent for 1,110 MBq (30 mCi) of ^{99m}Tc-EC-DG (i.e., the same as that typically administered for a ^{99m}Tc bone scan) would be 6.89 mSv. This compares to 9.99 mSv for a nominal 370 MBq (10 mCi) of an ^{18}F-FDG PET scan [22]. ^{99m}Tc-EC-DG had acceptable biodistribution, and did accumulate in the primary tumor of all six patients with confirmed NSCLC and concordant accumulation of ^{18}F-FDG (visualized best in the 4-h SPECT scans in this study). In addition, the administration of ^{99m}Tc-EC-DG was well tolerated in this cohort of patients.

Conclusion

The novel radiopharmaceutical ^{99m}Tc-EC-DG appears to be safe and to have acceptable dosimetric and biodistribution properties for a diagnostic nuclear medicine imaging agent. This conclusion is based on the lack of serious adverse reactions, a biodistribution not unusual for a diagnostic radiopharmaceutical and to some extent similar to that of ^{18}F-FDG, an effective dose equivalent similar to that of ^{99m}Tc-methylene diphosphonate (MDP) (6.10×10^{-3} mSv/MBq) and less than that of ^{18}F-FDG (3.00×10^{-2} mSv/MBq), and tumor uptake three to four times that in normal tissue. Larger studies are planned to further evaluate the diagnostic potential of this agent.

Acknowledgments We gratefully acknowledge the efforts of the following individuals: manager Anne Stachowiak; research nurses Deidre Mooring and Barbara Cacho; research administrator Jonathan Tinker, and administrative assistants Sylvia Kolojaco, Marie Turner, and Eloise Daigle; programmer analyst Mary Jane Oswald; Delta Polk, RN; research data coordinator Tina K. Peters; pathologists Nelson G. Ordonez, MD, and Adel K. El-Naggar, MD, PhD; cardiologist Joseph Swafford, MD; diagnostic radiologist Jeremy Erasmus, Jr., MD; physicists Osama Mawlawi, PhD, and Mohammed Salehpour, PhD; experimental nuclear medicine postdoctoral fellow Saady Kohanim, M.D.; and biostatistician Lyle D. Broemeling, PhD. We also thank Drs.

David C. Rice, Garrett L. Walsh, and chairman Jack A. Roth, for the continued support and referral of patients from the cardiovascular and thoracic service at M. D. Anderson Cancer Center.

This work was supported by a grant from Cell>Point LLC (Englewood, CO). We thank Greg Colip, Terry Colip, and Jerry Bryant, for their support of this project.

Conflicts of interest None.

References

1. Nolop KB, Rhodes CG, Brudin LH. Glucose utilization in vivo by human pulmonary neoplasm. Cancer 1987;60:2682–9.
2. Patz EFJ, Goodman PC. Positron emission tomography imaging of the thorax. Radiol Clin North Am 1994;32:811–23.
3. Nestle U, Walter K, Schmidt S, Licht N, Nieder C, Motaref B, et al. 18F-deoxyglucose positron emission tomography (FDG-PET) for the planning of radiotherapy in lung cancer: high impact in patients with atelectasis. Int J Rad Oncol Biol Phys 1999;44:593–7.
4. Mah K, Caldwell CB, Ung YC, Danjoux CE, Balogh JM, Ganguli SN, et al. The impact of 18FDG-PET on target and critical organs in CT-based treatment planning of patients with poorly defined non-small cell lung carcinoma: a prospective study. Int J Radiat Oncol Biol Phys 2002;52:339–50.
5. Yoo IeR, Park HJ, Hyun J, Chung YA, Sohn HS, Chung SK, et al. Two cases of pulmonary paragonimiasis on FDG-PET CT imaging. Ann Nucl Med 2006;20:311–5.
6. Sasaki M, Ichiya K, Kuwabara Y, Otsuka M, Tahara T, Fukumura T, et al. Ringlike uptake of 18F-FDG in a brain abscess: a PET study. J Comput Assist Tomogr 1990;13:829–31.
7. Gambhir SS, Czernin J, Schwimmer J, Silvermann DHS, Coleman RE, Phelps ME. A tabulated summary of the FDG PET literature. J Nucl Med 2001;42:1S–93S.
8. Kubota R, Yamada S, Kubota K, Ishiwata K, Tamahashi N, Ido T. Intratumoral distribution of F-18 fluorodeoxyglucose in vivo: high accumulation in macrophages and granulation tissues studied by microautoradiography. J Nucl Med 1992;33:1972–80.
9. Yang DJ, Kim CG, Schechter NR, Azhdarinia A, Yu DF, Oh CS, et al. Imaging with 99mTc ECDG targeted at the multifunctional glucose transport system: feasibility study with rodents. Radiology 2003;226:465–73.
10. Marshall S, Bacote V, Traxinger RR. Discovery of a metabolic pathway mediating glucose-induced desensitization of the glucose transport system. J Chem 1991;266:4706–12.
11. Wells L, Gao Y, Mahoney JA, Vosseller K, Chen C, Rosen A, et al. Dynamic O-glycosylation of nuclear and cytosolic proteins: further characterization of the nucleocytoplasmic beta-N-acetylglucosaminidase, O-GlcNAcase. J Biol Chem 2002;277:1755–61.
12. Pal S, Claffey KP, Cohen HT, Mukhopadhyay D. Activation of Sp1-mediated vascular permeability factor/vascular endothelial growth factor transcription requires specific interaction with protein kinase C zeta. J Biol Chem 1998;273:26277–80.
13. Black AR, Black JD, Azizkhan-Clifford J. Sp1 and krüppel-like factor family of transcription factors in cell growth regulation and cancer. J Cell Physiol 2001;188:143–60.
14. Yang DJ, Yukihiro M, Yu DF, Ito M, Oh CS, Kohanim S, et al. Assessment of therapeutic tumor response using 99mTc-ethylenedicysteine-glucosamine. Cancer Biother Radiopharm 2004;19:444–58.
15. Erwin WD, Groch MW, Macey DJ, DeNardo GL, DeNardo SJ, Shen S. A radioimmunoimaging and MIRD dosimetry treatment planning program for radioimmunotherapy. Nucl Med Biol 1996;23:525–32.
16. Siegel JA, Thomas SR, Stubbs JB, Stabin MG, Hays MT, Koral KF, et al. MIRD pamphlet no. 16: Techniques for quantitative radiopharmaceutical biodistribution data acquisition and analysis for use in human radiation dose estimates. J Nucl Med 1999;40:37S–61S.
17. Erwin WD, Groch MW, Spies SM. Development of a quantitative imaging and MIRD dosimetry software application for radionuclide therapy treatment planning using a fourth generation language (abstract). Radiology 1997;205(Suppl):261.
18. Erwin WD, Groch MW, Spies SM, Cutrera P, Groch PJ. Clinical validation of a quantitative imaging and MIRD dosimetry software application: retrospective application to anti-B-cell lymphoma MAB studies (abstract). Clin Nucl Med 1998;23:561.
19. Loevinger R, Budinger TF, Watson E; Medical Internal Radiation Dose Committee. MIRD primer for absorbed dose calculations. New York: The Society for Nuclear Medicine; 1991.
20. Stabin MG. MIRDOSE: personal computer software for internal dose assessment in nuclear medicine. J Nucl Med 1996;37:538–46.
21. Giraud I, Rapp M, Maurizis JC, Madelmont JC. Application to a cartilage targeting strategy: synthesis and in vivo biodistribution of 14C-labeled quaternary ammonium-glucosamine conjugates. Bioconjug Chem 2000;11:212–8.
22. International Commission on Radiation Protection. Radiation dose to patients from radiopharmaceuticals, ICRP Publ. No. 53. New York: Pergamon Press; 1988. p. 75–6.